DRAFT VERSION OCTOBER 14, 2015
Preprint typeset using LaTeX style emulateapj v. 01/23/15

arXiv:1510.03427v1 [astro-ph.EP] 12 Oct 2015

PHOTOPHORESIS IN A DILUTE, OPTICALLY THICK MEDIUM AND DUST MOTION IN PROTOPLANETARY DISKS

COLIN P. MCNALLY[1] AND ALEXANDER HUBBARD[2]

Draft version October 14, 2015

ABSTRACT

We derive expressions for the photophoretic force on opaque spherical particles in a dilute gas in the optically thick regime where the radiation field is in local thermal equilibrium. Under those conditions, the radiation field has a simple form, leading to well defined analytical approximations for the photophoretic force that also consider both the internal thermal conduction within the particle, and the effects of heat conduction and radiation to the surrounding gas. We derive these results for homogeneous spherical particles; and for the double layered spheres appropriate for modeling solid grains with porous aggregate mantles. Then, as a specific astrophysical application of these general physical results, we explore the parameter space relevant to the photophoresis driven drift of dust in protoplanetary disks. We show that highly porous silicate grains have sufficiently low thermal conductivities that photophoretic effects, such as significant relative velocities between particles with differing porosity or levitation above the midplane, are expected to occur.

Keywords: circumstellar matter — protoplanetary disks — planetary systems: formation — radiative transfer

1. INTRODUCTION

Photophoresis (Ehrenhaft 1918) is a set of phenomena where an incident flux of light drives particle motion though a gas by interaction with the gas molecules. In so-called 'ΔT_s-photophoresis', or thermo-photophoresis, illumination results in a thermal gradient across the grain. As a result, gas molecules recoil from the hot side of the dust grain more violently than they bounce off the cold side, generating a net force. Given sufficiently uniform surface properties and thermal conductivity within the particle, the side of the particle that sees a greater incident light flux will be hotter than the opposite side, even in the face of internal thermal conductivity within the particle and thermal conduction to the surrounding gas. In this scenario positive photophoresis results, pushing the dust grain away from the source of illumination.

Most of the photophoresis literature in astrophysics covers the case of direct illumination, which only formally applies in an optically thin medium. This is also the case for literature discussing photophoresis in the context of protoplanetary disk, which has to date primarily focussed on the transport of dust grains in optically thin regions of the disk illuminated by the proto-star. However, many sections of protoplanetary disks and other astrophysical environments are optically thick, so the basic formulation must be extended to cover those environments.

Moreover, recent work has shown that turbulent energy dissipation in the accretion disk context is highly localized, resulting in strong spatial temperature fluctuations insulated by high optical depths (McNally et al. 2014). Such hot spots are associated with radiative fluxes which drive photophoresis forces: in effect, a dust grain sees, not its immediate environment, but rather a bubble approximately an optical depth in radius whose surface temperature can vary meaningfully. The optically thick regime of photophoresis is the appropriate theory for deriving the forces and drift speeds of dust in such an environment.

cmcnally@nbi.dk
ahubbard@amnh.org
[1] Niels Bohr International Academy, Niels Bohr Institute, University of Copenhagen, Blegdamsvej 17, 2100 Copenhagen Ø, Denmark
[2] American Museum of Natural History, New York, NY, USA

Attention was drawn to the to the possible role of photophoresis in protoplanetary disks by Krauss & Wurm (2005), focusing primarily on the late, optically thin, stages of protoplanetary disk evolution. Photophoretic drift of particles in a protoplanetary disk has been studied in the context of disks which are sufficiently transparent for the direct illumination from the star to be dominant at the midplane (Mousis et al. 2007; Moudens et al. 2011). Wurm & Haack (2009a) examined photophoresis driven dust levitation in a protoplanetary disk, but applied the optically thin approach with a radiation source located at the disk midplane, and in Wurm & Haack (2009b) proposed that photophoresis can levitate CAIs above the disk in the optically thin region during an FU Ori outburst. In a work immediately preceding this one, Loesche et al. (2015), the scope for photophoresis was expanded to temperature fluctuations within the body of a protoplanetary disk, albeit in a formally one-dimensional treatment. In the atmospheres of accreting giant planets, photophoresis, even in the optically thick regime, can levitate and push out dust grains, limiting the opacity and accelerating the formation of these planets (Teiser & Dodson-Robinson 2013).

The dust grain's thermal conductivity is a central parameter in determining the photophoretic force. High conductivity reduces the internal thermal gradients and hence the effectiveness of photophoresis; and existing studies of photophoresis in protoplanetary disks considered specifically the difference between silicate and metal dust grain conductivities (Wurm et al. 2013). Solid particles which acquire a porous mantle of uncompacted dust with low conductivity will experience enhanced photophoresis (Loesche & Wurm 2012).

In this paper, we extend the optically thin direct illumination framework of photophoresis to the optically thick limit, including the effect of thermal conduction with the ambient gas as well as the impact of concentric shells with different thermal conductivities. Gratifyingly, all these disparate factors can be wrapped into a simple and powerful analytical closed form for the photophoretic forces and drift velocities. As an application, we consider dust motions in protoplanetary disks and show that the vastly differing thermal conductivities of highly porous and highly compacted dust grains cause a meaningful distinction between the effectiveness of

photophoresis for those grains. In inner regions of protoplanetary disks, we find that photophoresis can dominate over radial drift as a driver of collisions. Finally, we suggest that photophoresis driven by the release of accretion energy deep in the disk can levitate particles to several scale heights in a protoplanetary disk.

2. THEORY OF PHOTOPHORERSIS IN A DILUTE, OPTICALLY THICK MEDIUM

We concern ourselves with so-called 'ΔT-photophoresis', or thermo-photophoresis, arising from variation in the particle surface temperature T_s; as opposed to a photophoresis force resulting from any variation over the surface of the thermal accommodation coefficient α (which measures the rate with which gas molecules thermally equalize with the surface as they impinge upon it). We also restrict our attention here to opaque particles with a size greater than the wavelength corresponding to the temperature of the radiation field, so the photophoresis is positive (in the direction of the net light flux). Furthermore the theory that we derive shall be applicable in the limit that the particle surface temperature is close to the surrounding gas temperature. Finally, for simplicity, we assume perfect blackbody absorptivities and emissivities. Non-perfect blackbodies will have equally weaker radiation heating and cooling terms, increasing the relative effectiveness of the internal thermal conductivity and heat conduction to the gas.

In the free molecular flow regime, which we term 'dilute' and which is characterised by a Knudsen number > 1, the photophoresis force is generated by the momentum of particles impinging on the surface and re-emerging (Rohatscheck & Zulehner 1985; Rohatscheck 1995):

$$F_p = -\frac{1}{2}\oint_S p\left(1+\sqrt{\frac{\tilde{T}}{T_g}}\right)dS, \tag{1}$$

$$\tilde{T} \equiv T_g + \alpha(T_s - T_g), \tag{2}$$

where p is the background pressure, T_g is the background gas temperature, α is the thermal accommodation coefficient of the particle surface at temperature T_s, and the integral is taken over the surface of a particle. Of the above quantities, T_s, T_g, p, and α, we assume that only T_s (and hence $\tilde{T}$) varies across the particle's surface.

As in Rohatscheck & Zulehner (1985) we note that the position-independent part of the integral does not contribute, and linearize the square root in the limit

$$\zeta \equiv \frac{\alpha}{2}(T_s/T_g - 1) \ll 1. \tag{3}$$

Expanding, to linear order we have

$$\sqrt{1+2\zeta} = 1 + \zeta + \mathrm{O}\left(\zeta^2\right). \tag{4}$$

Because α is a constant of order unity, in practice this approximation is that $T_s/T_g - 1 \ll 1$, i.e. that the particle surface temperature is close to the surrounding gas temperature. To help sustain that approximation, we restrict ourselves to systems with sufficiently slowly spatially varying gas temperature that the temperature field can be treated as linear out to several optical depths.

We choose a coordinate system with the z-axis anti-aligned with any temperature gradient in the gas; and a spherical coordinate system with the pole ($\theta = 0$) aligned with the z-axis. For a sphere of radius a, Equation (1) then reduces to

$$F_p \cdot \hat{\boldsymbol{e}}_z = -\frac{1}{2}\int_0^{2\pi}\int_0^{\pi} p\left(2+\frac{\alpha}{2}\left(\frac{T_s}{T_g}-1\right)\right)a^2\cos(\theta)\sin(\theta)d\theta d\varphi. \tag{5}$$

If the particle surface temperature T_s is expressed as a Legendre series

$$T_s(\theta) = \sum_{n=0}^{\infty} A_n a^n P_n(\cos(\theta)), \tag{6}$$

then Equation (5) yields

$$F_p = -\frac{\pi}{3}\alpha\frac{p}{T_g}a^3 A_1 \hat{\boldsymbol{e}}_z. \tag{7}$$

This form for the photophoresis force on the sphere is commonly employed, and a significant part of the literature deals with approximations for A_1 (Beresnev et al. 1993; Rohatscheck 1995; Loesche & Wurm 2012).

2.1. *Intensity Field in an Optically Thick Medium*

The frequency-dependent intensity field to linear order in an optically thick medium with the temperature varying along the z-axis is given by

$$I_\nu(z,\mu) \approx B_\nu(T_g) - \frac{\mu}{\alpha_\nu+\sigma_\nu}\frac{\partial B_\nu(T_g)}{\partial T_g}\frac{\partial T_g}{\partial z} + \mathrm{O}(z^2), \tag{8}$$

where $\mu = \cos(\theta)$, $B_\nu(T_g)$ is the Planck function, and α_ν and σ_ν are the absorption and scattering opacities (Rybicki & Lightman 1986). Introducing the Rosseland Mean Opacity as

$$\frac{1}{\kappa_R\rho_g} \equiv \frac{\int_0^\infty(\alpha_\nu+\sigma_\nu)^{-1}\frac{\partial B_\nu}{\partial T}d\nu}{\int_0^\infty\frac{\partial B_\nu}{\partial T}d\nu}, \tag{9}$$

and integrating over frequency ν, the frequency-integrated intensity field near $z = 0$ is then given by

$$I(\theta) = \frac{\sigma_{SB}T_g^4}{\pi}\left[1+4\Gamma\cos\theta\right], \tag{10}$$

$$\Gamma \equiv -\frac{1}{\kappa_R\rho_g}\frac{\partial \ln T_g}{\partial z}. \tag{11}$$

This nondimensional parameter Γ is therefore the important control parameter in the theory. In an optically thick medium, one would expect that typically $\Gamma \lesssim 1$ as a steeper gradient would be rapidly smoothed by radiative thermal diffusion.

2.2. *Incident Intensity on a Small Sphere*

To determine the temperature structure of a sphere we need to integrate the incident intensity visible from any given point of the sphere's surface. Here we make use the the assumption that the sphere is opaque, and that the sphere has a size significantly larger than the wavelength corresponding to the temperature of the optically thick radiation field. Thanks to azimuthal symmetry around the z-axis for a sphere centered on the origin, calculating the incident intensity on the circle defined by intersection of the sphere with the yz plane suffices. Motivated by the fact that the x-axis is perpendicular to that circle, we will recalculate the intensity (Equation 10) in a spherical coordinate system with the x-axis as its pole.

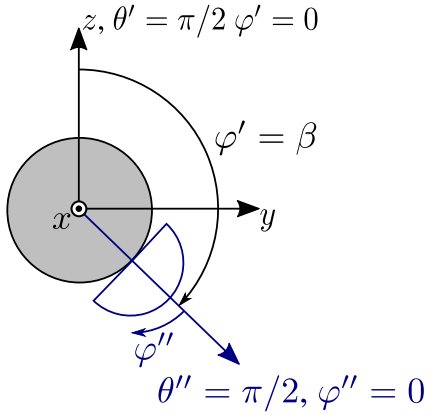

Figure 1. Geometry for the integral of incident intensity over the surface of a sphere

Noting further that this intensity is unchanged by a spatial translation, we define additional coordinate systems which are merely translations of the second coordinate system that place their origins on the circle. The angle between the surface and the radiation field, and appropriate limits of integration for the incident intensity are then straightforward to determine.

As planned, we first rewrite the intensity field in a new coordinate system, obtained by rotating the original one about the y axis, with the $\theta' = \pi/2$, $\varphi' = 0$ axis directed along z, and the pole ($\theta' = 0$) lying along the x axis. In this coordinate system, Equation (10) becomes

$$I(\theta', \varphi') = \frac{\sigma_{SB}}{\pi} T_g^4 [1 + 4\Gamma \sin\theta' \cos\varphi']. \tag{12}$$

Now translate this second coordinate system along ($\theta' = \pi/2, \varphi' = \beta$) to the surface of the sphere, to form a third coordinate system with $\theta'' = \theta'$, and $\varphi'' = 0$ corresponding to $\varphi' = \beta$, requiring that $\beta \leq \pi$. Note specifically that the poles of the second and third coordinate systems are aligned, and that the pole of the third coordinate system is tangent to the sphere. As shown in Figure 1, for $\theta'' = \pi/2$, we have $\beta = \theta$ from the original coordinate system. Because of the azimuthal symmetry around the radiation field, the incident flux on any point on a sphere defined through ($\theta = \beta, \varphi \in [0, 2\pi]$) in the original coordinate system is the same as the incident flux on the oriented point defined through ($\theta'' = \pi/2, \varphi'' = 0$) in the third coordinate system.

We now integrate over the solid angle visible from the point defined through ($\theta'' = \pi/2, \varphi'' = 0$). The projection of a ray direction onto the surface normal $\hat{n}$ is $\sin\theta'' \cos\varphi''$, and we require the projection of each inwards going ray (for each visible direction $\beta + \varphi''$ the ray incoming along $\beta + \varphi'' + \pi$) onto the inward directed surface normal $-\hat{n}$. Further, by construction both the pole ($\theta'' = 0$) and the vector ($\theta'' = \pi/2, \phi'' = \pi/2$) are tangent to the sphere's surface, which sets the limits of integration. The integral for the incident intensity on the surface of a small sphere is therefore

$$I_n(\beta) = \int_{\text{outward}} I(\theta'', \varphi'') \cdot (-\hat{n})\, d\Omega \tag{13}$$

$$= \int_0^{\pi} \int_{-\pi/2}^{\pi/2} I(\theta'', \beta + \varphi'' + \pi) \sin\theta'' \cos\varphi'' \times \sin\theta'' d\varphi'' d\theta'' \tag{14}$$

$$= \sigma_{SB} T_g^4 \left[1 - \frac{8}{3}\Gamma \cos(\beta)\right]. \tag{15}$$

This intensity is then the forcing on the boundary for the heat transfer calculation in the sphere, which will yield the variation of the particle surface temperature T_s.

2.3. *Surface Temperature of an Irradiated Sphere*

To solve the problem of the heat transfer within a spherical particle we make several assumptions. First, we include both thermal conduction to the gas, and thermal radiation from the particle surface. The conductive heat flux away from the surface in a dilute gas given by Stoffels et al. (1996):

$$I_c = \Upsilon T_g^{1/2} (T_g - T_s), \tag{16}$$

$$\Upsilon \equiv \frac{\gamma + 1}{8(\gamma - 1)} \alpha \sqrt{\frac{2}{\pi}} \left(\frac{k_B}{\mu m_H}\right)^{3/2} \rho_g. \tag{17}$$

Second, we shall assume that the particle is opaque such that the irradiation imparts energy only on the spherical surface of the particle, and not inside the volume. This breaks down for small, low volume filling fraction particles which might only have one or two monomers along a given ray through the particle.

Under these assumptions the heat equation within the sphere is simply Laplace's equation $\nabla^2 T = 0$, and the solution can can be expressed as a series in $r^\ell P_\ell(\cos\theta)$ where the P_ℓ are Legendre polynomials. The coefficients of the solution are obtained by solving the boundary condition equating the flux of energy conducted from the surface and radiated from the surface to the incident energy:

$$k \left.\frac{\partial T(r,\theta)}{\partial r}\right|_a + \sigma_{SB} T(a,\theta)^4 - I_c(\theta) = I_n(\theta), \tag{18}$$

where $T(r, \theta)$ is the internal temperature of the particle, k its thermal conductivity and a is its radius. We decompose the particle temperature into a constant component and a spatially varying one:

$$T(r, \theta) = T_0 + T'(r, \theta). \tag{19}$$

We linearize the problem with the small parameter being the deviation of the particle temperature

$$\eta = T'(r, \theta)/T_0 \ll 1. \tag{20}$$

The linearized problem is then

$$k \left.\frac{\partial T'}{\partial r}\right|_a + \sigma_{SB} T_0^4 \left(1 + \frac{T'}{T_0}\right)^4 - \Upsilon T_g^{1/2} \left(T_g - T_0 \left(1 + \frac{T'}{T_0}\right)\right) = \sigma_{SB} T_g^4 \left[1 - \frac{8}{3}\Gamma \cos(\theta)\right]. \tag{21}$$

By expanding the second term on the left hand side to linear order in η and substituting a Legendre series for T we obtain the solution in terms of the first two terms of the Legendre series:

$$T_0 = T_g \tag{22}$$

and

$$T'(r,\theta) = A_1 r\cos(\theta) + \mathrm{O}\left[(A_1 a)^2\right], \tag{23}$$

$$A_1 = -\frac{8}{3}\frac{\sigma_{SB}T_g^4\Gamma}{k}\left(1 + 4\sigma_{SB}T_g^3\frac{a}{k} + \Upsilon T_g^{1/2}\frac{a}{k}\right)^{-1}. \tag{24}$$

In Appendix A we compare this to a solution of the full problem to verify the validity of the linear approximation in the protoplanetary disk regime.

Combining Equations (3), (19), (22), (23) and (24) we find

$$\zeta = -\frac{8}{3}\alpha\sigma_{SB}T_g^3\Gamma\frac{a}{k}\left(1 + 4\sigma_{SB}T_g^3\frac{a}{k} + \Upsilon T_g^{1/2}\frac{a}{k}\right)^{-1}\cos(\theta). \tag{25}$$

For the $\zeta \ll 1$ expansion of the force integral to hold to linear order, we need one or a combination of $\Gamma \ll 1$, $\Upsilon T_g^{1/2}\frac{a}{k} \gg 1$, or $\sigma_{SB}T_g^3\frac{a}{k} \ll 1$.

At this point we can insert this result into Equation (7) to yield the photophoresis force as

$$F_p \approx \frac{8\pi}{9}\frac{k_B}{\mu m_H}\alpha\frac{a^3}{k}\rho_g\sigma_{SB}T_g^4\Gamma \left(1 + 4\sigma_{SB}T_g^3\frac{a}{k} + \Upsilon T_g^{1/2}\frac{a}{k}\right)^{-1}\hat{\boldsymbol{e}}_z\,. \tag{26}$$

where we have used $p = k_B\rho_g T_g/(\mu m_H)$. We proceed to examine several limiting cases where the form of the force can be usefully simplified.

2.3.1. *Limits*

As mentioned in the previous section, the validity of the $\zeta \ll 1$ expansion of the force integral requires one or a combination of $\Gamma \ll 1$, $\Upsilon T_g^{1/2}\frac{a}{k} \gg 1$, or $\sigma_{SB}T_g^3\frac{a}{k} \ll 1$. The first case does not lead to a significant simplification, and the second case leads to a very small photophoresis force. In the third case the photophoresis force on a single-layered spherical particle simplifies to

$$F_p \approx \frac{8\pi}{9}\frac{k_B}{\mu m_H}\alpha\frac{a^3}{k}\rho_g\sigma_{SB}T_g^4\Gamma\left(1 + \Upsilon T_g^{1/2}\frac{a}{k}\right)^{-1}\hat{\boldsymbol{e}}_z. \tag{27}$$

Furthermore, where the heat transfer by conduction from the particle to the gas is much smaller than the radiative cooling of the particle, the force further simplifies:

$$F_p \approx \frac{8\pi}{9}\frac{k_B}{\mu m_H}\alpha\frac{a^3}{k}\rho_g\sigma_{SB}T_g^4\Gamma\hat{\boldsymbol{e}}_z. \tag{28}$$

Equation (28) gives a force which is always greater than the more general form in Equation (26). In Section 2.7 we will determine where this difference becomes significant for a specific particle model.

2.4. *Surface Temperature of an Trradiated Double-layer Sphere*

As particles with outer rims of a material with differing thermal conductivity are of interest in protoplanetary disks we proceed now to develop a similar approximation for double layered particles. For a double-layer sphere with the same basic assumptions as for the single layer sphere, we develop the solution in terms of series expansions in the core and mantle ($T_c(r,\theta)$ and $T_m(r,\theta)$) layers as

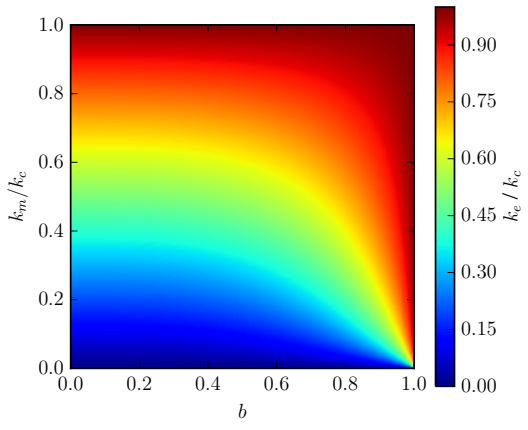

Figure 2. Equivalent conductivity k_e (Equation 34) of a double-layer sphere in terms of a single-layer sphere when radiation dominates the particle cooling and effective $\sigma_{SB}T_g^3\frac{a}{k} \ll 1$.

$$T_c(r,\theta) = \sum_{n=0}^{\infty}\left(C_n r^n\right)P_n(\cos(\theta)), \tag{29}$$

$$T_m(r,\theta) = \sum_{n=0}^{\infty}\left(A_n r^n + B_n r^{-n-1}\right)P_n(\cos(\theta)). \tag{30}$$

The boundary conditions at the core radius r_c match the energy flux and temperature between the core with thermal conductivity k_c and mantle with thermal conductivity k_m through

$$k_c\left.\frac{\partial T_c}{\partial r}\right|_{r_c} = k_m\left.\frac{\partial T_m}{\partial r}\right|_{r_c}, \tag{31}$$

$$T_c(r_c,\theta) = T_m(r_c,\theta), \tag{32}$$

where the second equation assumes that the interface has perfect conduction. At the exterior, mantle plus core radius a, the boundary condition is again Equation (18) although with the mantle's thermal conductivity k_m.

The linear approximation in $\eta \ll 1$ for this problem and its solution are given in Appendix B. The result for the photophoresis force on a double-layered sphere in a dilute optically thick medium is:

$$F_p \approx \frac{8\pi}{9}\frac{k_B}{\mu m_H}\alpha\frac{a^3}{k_m}\rho_g\sigma_{SB}T_g^4\Gamma\left[(1-b^3) + \frac{k_m}{k_c}(2+b^3)\right] \times\left[2\frac{k_m}{k_c}(1-b^3) + \left(1+2b^3\right) + \frac{a}{k_m}\left((1-b^3) + \frac{k_m}{k_c}(2+b^3)\right)\left(\Upsilon T_g^{1/2} + 4\sigma_{SB}T_g^3\right)\right]^{-1}\hat{\boldsymbol{e}}_z, \tag{33}$$

where $b = r_c/a$ is the radius of the core in terms of the exterior radius of the sphere.

Comparing Equation (33) with Equation (26) in the case that radiative cooling dominating over conductive cooling, requiring additionally $\sigma_{SB}T_g^3\frac{a}{k_m} \ll 1$, gives the equivalent single-layer conductivity of a double-layered sphere with the

same meaning as given for the optically thin case by Loesche & Wurm (2012):

$$k_e = k_m \left[(1-b^3) + \frac{k_m}{k_c}(2+b^3) \right]^{-1} \times \left[2\frac{k_m}{k_c}(1-b^3) + \left(1+2b^3\right) \right]. \quad (34)$$

This is illustrated in Figure 2, showing that mantle layers of low conductivity material do dramatically alter the effective property of a particle with $b \lesssim 5/6$.

2.5. *Photophoresis Drift Velocity*

The drag force $\boldsymbol{F}_d$ is the aerodynamic drag on particles, and can be written as

$$\boldsymbol{F}_d = -m_d \frac{\boldsymbol{v}}{\tau}, \quad (35)$$

where τ is the particle frictional stopping time. It will be useful to define the particle Stokes number

$$St \equiv \tau \Omega_K \quad (36)$$

where Ω_K is the local Keplerian frequency .

In practice, small, sub-centimeter particles in protoplanetary disks are in the 'free molecular flow' regime, i.e. the Epstien drag regime. From Blum et al. (1996)'s experiments on the Brownian motion diffusion of particles, under these conditions Equation (35) takes the form

$$\boldsymbol{F}_d = -\frac{\sigma_a \rho_g v_g}{\epsilon}\boldsymbol{v}, \quad (37)$$

with $\epsilon = 0.68$ an experimentally determined constant, v_g the mean thermal speed of gas particles

$$v_g = \sqrt{\frac{8k_B T_g}{\pi \mu m_H}}, \quad (38)$$

and $\sigma_a = \pi a^2$ the geometric cross section of the particle.

Balancing the drag force and the photophoresis force in the approximation of Equation (26) gives a drift speed of

$$v_p = \frac{1}{9}\sqrt{\frac{8\pi k_B}{\mu m_H}}\,\epsilon\alpha\frac{a}{k}\sigma_{SB}T_g^{7/2}\Gamma \times \left(1 + 4\sigma_{SB}T_g^3\frac{a}{k} + \Upsilon T_g^{1/2}\frac{a}{k}\right)^{-1}. \quad (39)$$

2.6. *When does photophoresis dominate over radiation pressure?*

In SI units the force due to radiation pressure on a black sphere with radius a is:

$$F_r = \frac{I}{c}\pi a^2, \quad (40)$$

and here the Rosseland mean flux can be used for I, as the relevant quantity is the net momentum of the photons impacting the particle. Following Rybicki & Lightman (1986) we write

$$I = \frac{16}{3}\sigma_{SB}T_{\rm g}^4\Gamma\hat{\boldsymbol{e}}_z. \quad (41)$$

Treating the drag force in the same manner as with photophoresis, the resulting drift speed of the particle is

$$v_r = \frac{18}{3}\sqrt{\frac{\pi\mu m_H}{8k_B}}\frac{\epsilon}{c\rho_g}\sigma_{SB}T_g^{8/2}\Gamma. \quad (42)$$

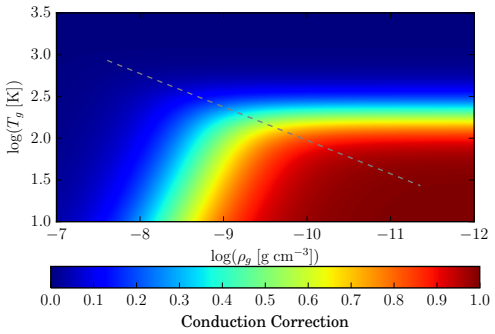

Figure 3. Conduction correction for a very porous 1 mm silicate aggregate particle with accordingly very low thermal conductivity 1.5×10^2 erg s^{-1}cm^{-1}K^{-1}. The dashed curve is the MMSN midplane density and temperature.

Due to the linear nature of the Epstien drag regime, the drift velocities due to the two forces simply add linearly. Accordingly, the ratio between the drift speeds is

$$\frac{v_p}{v_r} = \frac{1}{54}\frac{8k_B}{\mu m_H}c\rho_g\alpha\frac{a}{k}T_g^{-1}\left(1 + 4\sigma_{SB}T_g^3\frac{a}{k} + \Upsilon T_g^{1/2}\frac{a}{k}\right)^{-1}, \quad (43)$$

where Equation (26) has been used for the photophoresis force to ensure generality across parameter space. Radiation pressure dominates at low density, high temperature and high conductivity. These parameters fall mainly outside the regime of the optically thick part of a protoplanetary disk. However, if desired, the combined drift velocity of dust due to photophoresis and radiation pressure in a dilute optically thick medium can be obtained from the formulas already given in this work.

2.7. *When can heat transfer by conduction be neglected?*

The question at hand is when does Equation (28) provide a good approximation to Equation (26)? The latter always yields a smaller force, so when the approximation ceases to hold the photophoresis force is effectively shut off. For the sake of this discussion, we refer to the factor

$$\left(1 + 4\sigma_{SB}T_g^3\frac{a}{k} + \Upsilon T_g^{1/2}\frac{a}{k}\right)^{-1} \quad (44)$$

in the photophoretic force for a sphere as given by Equation (26) as the 'conduction correction'. Figure 3 gives this conduction correction for a 1 mm particle with conductivity 1.5×10^2 erg s^{-1}cm^{-1}K^{-1}. The iso-countours of this plot are roughly two power-laws, breaking coincidentally around the MMSN midplane density-temperature relation. It can be roughly said that below the break the contour is set by the effect of heat conduction to the surrounding gas ($\Upsilon T_g^{1/2}a/k$), while above the break it is set by the $4\sigma_{SB}T_g^3 a/k$ term.

In Figure 4 a more general result is plotted, with curves of the critical contour in T_g-ρ_g space where the difference between Equation (28) and Equation (26) is 50%. For large, porous particles, which otherwise have the largest photophoresis forces the conduction terms have the most dramatic effect in shutting down photophoresis.

3. APPLICATIONS IN PROTOPLANETARY DISKS

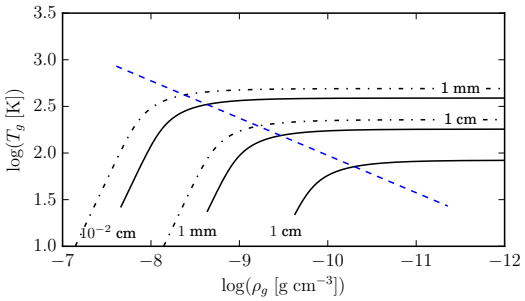

Figure 4. Contours where the extra conduction terms decrease the photophoresis force by a factor of 50%. Contours are are labelled with particle radius a, and to the left and above of each contour conduction has reduced the photophoresis force by more than half. Solid lines are for particles with volume filling factor $\phi = 0.12$ and dash-dot lines are for particles with $\phi = 0.5$.

3.1. *Particle Model*

For the purposes of estimating the effects of photophoresis in a protoplanetary disk, we adopt a model of particles following from the experimental measurements of the thermal conductivity of packed silicate monomers by Krause et al. (2011). These give well constrained values of the thermal conductivity so vital to determining the photophoresis force, finding

$$k(\phi) = k_0 e^{7.91\phi}, \tag{45}$$

with

$$k_0 = 5.14 \times 10^{-4}\ \mathrm{W\ m^{-1}K^{-1}}, \tag{46}$$

or $k_0 = 51.4\ \mathrm{erg\ s^{-1}cm^{-1}K^{-1}}$. In Equation (45), ϕ is the grain's volume filling factor, defined for a given sample as $\phi \equiv \rho_d/\rho_0$ where ρ_d is the density of the bulk sample and ρ_0 the mass density of the constituent solid silicate monomers (Krause et al. 2011). Other grain materials, such as organics/graphite or mixed material grains are of great interest in planet formation, but such experimental data does not yet exist for those materials, so we only consider silicate particles, and vary the volume filling factor and radius of the particles.

For our model aggregates, a dust grain of mass m_d has a density and radius:

$$\rho_d = \phi \times \rho_0, \tag{47}$$

$$a = \left(\frac{3m_d}{4\pi\rho_0}\right)^{1/3} \phi^{-1/3}. \tag{48}$$

where $\rho_0 \simeq 3 \times 10^3\ \mathrm{kg\,m^{-3}}$ is the density of fused silicates of chondritic composition.

We assume for simplicity that non-thermally processed dust grains are composed of

$$a_0 = 0.75\ \mu\mathrm{m} \tag{49}$$

sized monomers (Güttler et al. 2010). For silicate dust, the results of Hubbard (2015) imply that thermal processing for micron sized grains occurs on several week timescales at $T = 900\,\mathrm{K}$ and several decade timescales at $T = 850\,\mathrm{K}$, and so for $T < 850\,\mathrm{K}$, a fluffy porous structure is expected, while for $T > 900\,\mathrm{K}$, the dust grains should be fused. We further normalize our grain masses to

$$m_{d0} = 2 \times 10^{-4}\ \mathrm{g} \simeq \frac{4\pi}{3}\rho_0 \times (0.25\ \mathrm{mm})^3, \tag{50}$$

the mass corresponding to a typical chondrule found in the LL3.0 chondrite Semarkona (Friedrich et al. 2014). In the application here, we consider that the particle has the same mean temperature as the gas at its location. For mm-size and smaller paticles in a protoplanetary disk, this is a reasonable assumption for timescales longer than minutes (Loesche et al. 2015).

3.2. *MMSN Model*

To examine particle motion in a protoplanetary disk we adopt the Hayashi minimum mass solar nebula (MMSN, Hayashi 1981) as our canonical disk model, with its temperature set by the stellar irradiation:

$$T_g = 270 R^{-1/2}\ \mathrm{K}, \tag{51}$$

$$\Omega_K = 2 \times 10^{-7} R^{-3/2}\ \mathrm{s^{-1}}, \tag{52}$$

$$H = \sqrt{\frac{p}{\rho_g}}\Omega_K^{-1}, \tag{53}$$

$$\rho_g = \rho_{g0} e^{-z^2/2H^2}, \tag{54}$$

$$\Sigma_g = \sqrt{2\pi}\rho_{g0} H = 1700 R^{-3/2}\ \mathrm{g\ cm^{-2}}. \tag{55}$$

T_g is the background disk temperature, Ω_K is the Keplerian orbital angular velocity, H is the scale height assuming vertical hydrostatic equilibrium, ρ_{g0} is the midplane gas volume density, Σ_g is the disk gas surface density, and R the orbital position measured in AU. We can rewrite Equation (53) as

$$\Omega_K^2 = \frac{p}{\rho_g} H^{-2} = \frac{k_B T_g}{\mu m_H} H^{-2}. \tag{56}$$

This provides the background in which we examine optically thick photophoresis. We follow Loesche et al. (2015) in assuming that the opacity in the medium is provided by small grains which can be assumed to be well-coupled to the temperature of the gas.

3.2.1. *Temperature Gradients*

McNally et al. (2014) is the only study of self-consistent heating and cooling of current sheets in a local simulation of a protoplanetary disk flow we are aware of at this time which allows the identification of maximal temperature variations and temperature gradients in the optically thick regime. Analyzing those simulations, we find that they contain well resolved temperature gradients with maximum Γ varying typically between $1 - 7 \times 10^{-4}$ over time. Hence, we take that result as an estimate for local temperature fluctuations in the analysis of protoplanetary disks, normalizing our results to a fiducial value of $\Gamma = 10^{-4}$. We caution that Γ is not known to be universal, and other disk flow regimes may have different typical maximal values of Γ. We hope that this work will motivate further studies characterizing other regimes.

3.3. *Particle Drift Speeds are Very Porosity Dependent*

Figure 5 shows photophoresis driven particle drift speeds for particles with mass 2×10^{-4} g and varying porosity. For these equal mass particles, the drift speeds vary greatly depending on the porosity. With our fiducial $\Gamma = 10^{-4}$ temperature gradient the speed differences are commonly an order of magnitude at the MMSN midplane and higher temperatures.

3.4. *Comparison to Radial Drift Speeds*

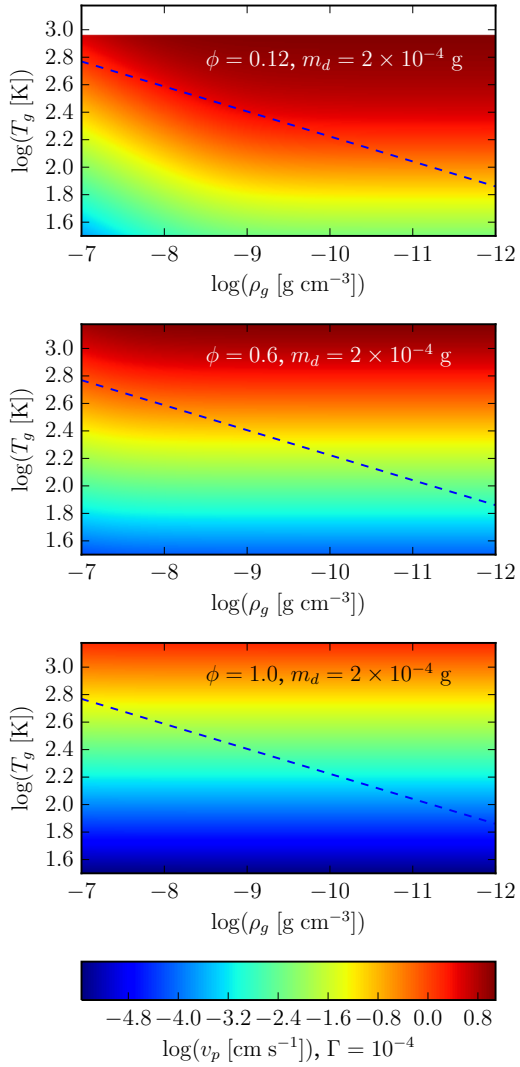

Figure 5. Photophoresis driven drift velocities (Equation (39) for particles of a fixed mass and varying porosity driven by a fluctuation with temperature gradient $\Gamma = 10^{-4}$. When solid, with $\phi = 1$, these particle have a radius of 1 mm. The dashed line gives the MMSN midplane density-temperature relation. In the upper panel, no data is shown above $T_g = 900$ K as silicate grains will rapidly compact at temperature similar to this, leaving no very porous grains at higher temperatures.

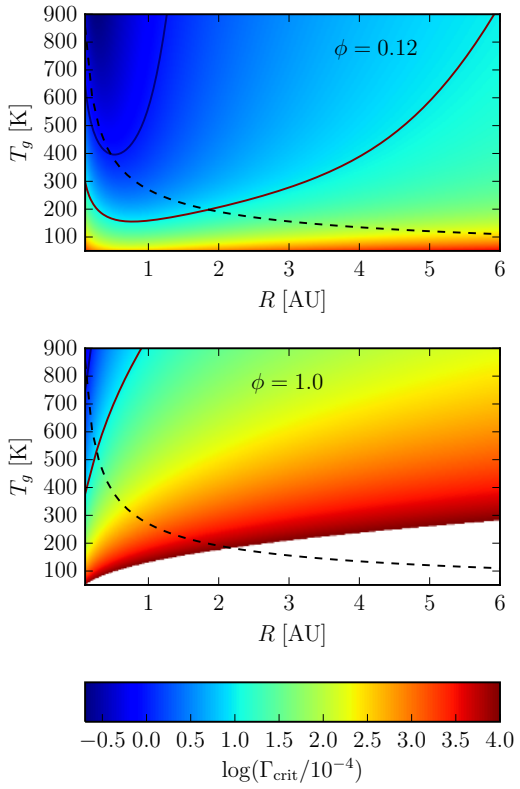

Figure 6. Critical temperature gradient $\Gamma_{\rm crit}$ for the photophoresis driven drift velocity to equal the radial drift velocity. Solid contours are drawn at $\Gamma_{\rm crit} = 10^{-4}, 10^{-3}$, and the values are cut off at $\Gamma_{\rm crit} > 1.0$. The dashed line shows the MMSN midplane temperature radius relation. This indicates that at small radii photophoresis driven collisions can dominate over radial drift driven collisions when $\Gamma \gtrsim 10^{-4}$, particularly for porous grains.

The photophoretic drift speed v_p depends on the particle's size and thermal conductivity (and hence its porosity). Two particles with different (a, ϕ) would therefore experience different drift speeds $v_p(a, \phi)$ even in the same gas environment. This results in a relative drift which can drive collisions with a speed comparable to the higher photophoretic drift speed of the two particles. We can check the relevance of photophoresis due to temperature fluctuations on particle collisions by comparing v_p to other dust drift speeds. The most common drift speed considered for collisions is dust settling, which is complicated in the presence of photophoresis due to photophoretic levitation (see Section 3.5). However dust also drifts radially.

This radial drift is due to the inwards pointing radial pressure gradient in protoplanetary disks, which causes the gas to orbit at a sub-Keplerian velocity. Inertial particles do not feel the pressure gradient and so orbit faster than the gas and feel a headwind which slows them, and causes them to gradual inspiral. Following Weidenschilling (1977) we write the orbital velocity of the gas as

$$u_g = (1 - \eta) u_K, \tag{57}$$

where

$$u_K = R\Omega_K \tag{58}$$

is the local Keplerian velocity and Ω_K the Keplerian frequency. In an MMSN with $T \propto R^{-1/2}$, we have $\eta \ll 1$, and $\eta u_K \simeq 45$ m s^{-1}, independent of the orbital position. We can write the radial velocity equation for particles well coupled to the gas (i.e. the particle's orbital velocity matches the gas) under the assumption that terminal radial velocity has been achieved (Equation 35):

$$\frac{\partial v_r}{\partial t} = -\frac{v_r}{\tau} + \frac{v_{orb}^2}{R} - \frac{u_K^2}{R} = 0. \tag{59}$$

Using Equation (36) we can write the equation for the headwind induced inspiral drift speed

$$v_r \simeq -2St\,\eta\,u_K. \tag{60}$$

Like photophoresis, this will drive collisions between particles with different drag coefficients.

Photophoresis from local temperature fluctuations will drive more powerful and frequent collisions if $|v_p| > |v_r|$,

i.e. if

$$\frac{\tau F_p}{m_d} > 2St\eta u_K. \quad (61)$$

From this, we can determine the critical value $\Gamma_{\rm crit}$ where photophoresis driven velocities equal the radial drift velocity at the midplane

$$\Gamma_{\rm crit} = 3\sqrt{\frac{2\pi\mu m_H}{k_B}}\frac{k}{\alpha\sigma_{SB}}\frac{\rho_0}{\Sigma_g}T_g^{-7/2} \left(1 + 4\sigma_{SB}T_g^3\frac{a}{k} + \Upsilon T_g^{1/2}\frac{a}{k}\right)\eta u_K \quad (62)$$

Figure 6 gives the size of temperature gradient due to local temperature fluctuations needed for photophoresis driven drift to equal the MMSN radial drift speed ($\eta u_K = 45\ {\rm m\ s^{-1}}$) for particles with small Stokes number. These are normalized to our fiducial value of $\Gamma = 10^{-4}$. In an MMSN, porous ($\phi = 0.12$) grains satisfy $\Gamma_{\rm crit} < 10^{-3}$ inwards of 2 AU, and $\Gamma_{\rm crit} < 10^{-4}$ inwards of 0.5 AU. Future studies of the appropriate parameter range for Γ are therefore needed for studies of collisional grain growth in the inner few AU of protoplanetary disks.

3.5. *Dust Levitation in a MMSN Protoplanetary Disk*

Here we find that levitation is also possible in the optically thick region of a quiescent disk for sufficiently porous grains, if the effective temperature due to accretion power is a significant fraction of the actual temperature several scale heights above the midplane. Photophoretic dust levitation is driven by the optically thick vertical flux of energy resulting from the dissipation of accretion energy deep in the disk. This flux can be parameterized in terms of the accretion power's contribution to the effective temperature of the disk as:

$$P(z) = \sigma_{SB}T_{\rm e,acc}^4(z). \quad (63)$$

where we denote this contribution as $T_{\rm e,acc}$ to explicitly note that it results from accretion power, not irradiation. At any given height h in the disk, $2F(z)$ is the vertically integrated accretion power released below that height $|z| < h$, where the factor of 2 accounts for the two sides of the disk. In this parameterization, $T_{\rm e,acc}$ is the effective temperature that the disk would have if the accretion power released below $|z| < h$ were the only energy source for the disk, and can be compared to the irradiation temperature.

Expressing the vertical energy flux E in terms of the optically thick flux using Equation (10) as

$$E = \int_0^{\pi}\int_0^{2\pi} I(\theta)\cos\theta\sin\theta d\phi d\theta = \frac{16}{3}\sigma_{SB}\Gamma T_g^4, \quad (64)$$

we find the the resulting temperature gradient must be

$$\Gamma = \frac{3}{16}\frac{T_e^4}{T_g^4}. \quad (65)$$

We will seek to balance the photophoresis force on a sphere Equation (26) against the gravitational force on a dust grain of mass m_d given as

$$F_g = -m_d z\Omega^2\hat{\boldsymbol{e}}_z. \quad (66)$$

Combining the above three equations with the equations for an MMSN we find that gravity and photophoresis balance at a critical effective temperature $T_{\rm e,crit}$ when

$$\frac{\pi}{6}\frac{k_B}{\mu m_H}\alpha\frac{a^3}{k}\rho_g\sigma_{SB}T_{\rm e,crit}^4\left(1 + 4\sigma_{SB}T_g^3\frac{a}{k} + \Upsilon T_g^{1/2}\frac{a}{k}\right)^{-1} = \frac{4\pi\phi\rho_0 a^3}{3}z\Omega^2. \quad (67)$$

Using Equation (56) we can simplify the above to

$$\frac{1}{8}\frac{\alpha}{k}\rho_g\sigma_{SB}T_e^4\left(1 + 4\sigma_{SB}T_g^3\frac{a}{k} + \Upsilon T_g^{1/2}\frac{a}{k}\right)^{-1} = \phi\rho_0 z\frac{T_g}{H^2}. \quad (68)$$

Rearranging terms and using Equations (54) and (55) we come to

$$\left(\frac{T_{\rm e,crit}}{T_g}\right)^4 = \frac{\sqrt{2\pi}8}{\sigma_{SB}T_g^3}\frac{\rho_0}{\Sigma_g}\frac{k\phi}{\alpha}\left(\frac{z}{H}e^{+z^2/2H^2}\right) \left(1 + 4\sigma_{SB}T_g^3\frac{a}{k} + \Upsilon T_g^{1/2}\frac{a}{k}\right), \quad (69)$$

where we note that Υ depends on both Σ_g and z/H through its dependence on ρ_g.

In Figure 7 we plot the critical effective temperature $T_{e,crit}$ such that Equation (69) is satisfied in an MMSN background. Our parameters are $R, z/H, \phi$, and a (and hence dust particle density m_d). We include contours of $\log(T_{\rm e,crit}/T_g) = -0.5$, at which level the accretion power would only be 1% of the background disk luminosity. That represents a very quiescent disk almost fully heated through irradiation, and is a conservative estimate for a level of accretion power that must be considered in any protoplanetary disk model.

In the top left panel of Figure 7 we show that for $\phi \lesssim 0.3$, porous dust grain up to approximately 1 mm in radius are highly subject to photophoretic levitation up to at least $z/H = 1$ at $R = 1$ AU; demonstrating the basic importance of considering photophoresis in terrestrial planet forming regions. In the top right panel we show that highly porous $\phi \lesssim 0.12$ grains are highly subject to photophoretic levitation out to at least $R = 2$ AU, and most likely into the asteroid belt region $R = 2 - 3$ AU; however, photophoresis requires significant levels of accretion power to play a major role farther out. In the bottom left panel we show the levitation profile for a dust grain with mass comparable to chondrules found in the LL3.0 chondrite Semarkona, with a radius $a \sim 0.25$ mm (Friedrich et al. 2014), demonstrating that chondrule precursors are likely to have been levitated away from the midplane. Finally, the bottom right panel shows that highly porous dust grains would have been levitated well above the midplane, to about $z/H \gtrsim 2$, until they grow past the $100\,\mu$m mark, at which point photophoretic levitation begins to be less effective (although it can still play a significant role for particles with $a \gtrsim 1$ mm).

In aggregate, Figure 7 demonstrates that photophoretic levitation is expected to play a major role in vertically distributing highly porous, collisionally grown dust in the terrestrial planet forming region of protoplanetary disk, out to the current location of the asteroid belts. However, as dust processing continues, the larger and more compacted grains would decouple from the photophoretic force; which could only play a role during accretion events such as FU Orionis outbursts, when we would expect $T_e > T$. In particular, we note that chondrule precursors are likely to have been levitated above the midplane.

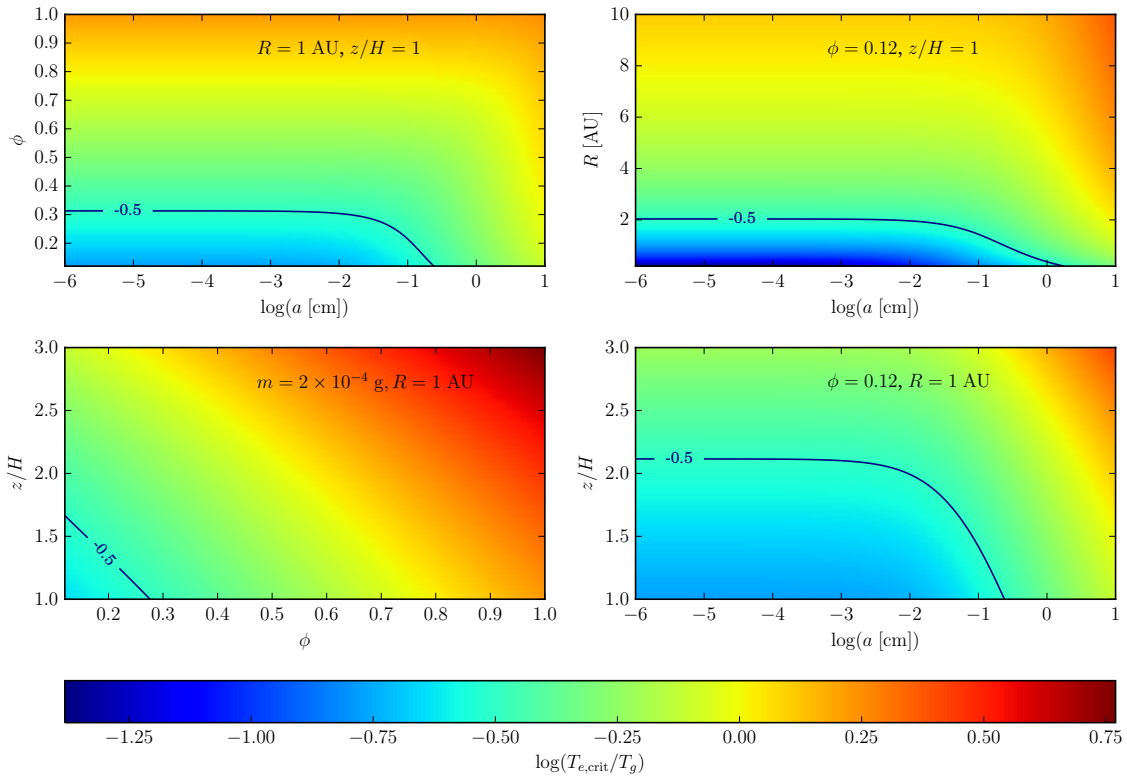

Figure 7. Critical effective temperature due to accretion heating $T_{\rm e,crit}$ which will produce dust levitation for various parameters. Plotted is the ratio $T_{\rm e,crit}/T_g$, where T_g is the actual local gas temperature, and the solid contours show an example level $\log(T_{\rm e,crit}/T_g) = -0.5$. Where is this condition is fulfilled by the disk structure the region below the contour would correspond to dust photophoretically levitated in the disk. *Upper Left:* as a function of radius a and porosity ϕ at 1 AU and at the height of one scale height in a MMSN. At this location, levitation cuts off for particles above $a \sim 1$ mm. *Upper Right:* as a function of particle radius a and radial position R for a fixed very low porosity ϕ at one scale height. We see that at small radial positions levitation may occur, but would result in only particles with $a \lesssim 1$ mm being levitated. *Lower Left:* For particles with the mass of a typical chondrule at 1 AU photophoresis has a weak ability to levitate, with the only possibility being for the most porous particles. *Lower Right:* At 1 AU small, porous particles may be levitated to several scale heights.

4. CONCLUSIONS

We have derived the general theory for photophoresis force on an opaque, homogeneous, spherical particle with either one or two layers in a dilute, optically thick medium. This analysis is simple and general, making no assumptions specific for protoplanetary disks. In itself, the theory presented here applies equally well to any astrophysical or terrestrial system with the same basic criteria.

The theory developed here for spherical grains shows that the effects are most pronounced for the lowest conductivity grains. However, those grains have that property because they are very porous. The assumptions of opaque spherical particles, used here and in Loesche & Wurm (2012), must break down at some point for sufficiently porous grains. Improving on this state of the art is clearly important future work.

In protoplanetary disks, photophoresis driven by accretion processes dissipating energy into heat can have dynamical impacts for highly porous grains, including levitating chondrule precursors mass objects above the midplane. This effect would rapidly decay as collisions or thermal processing compactify the grains. Photophoresis as a levitation effect in protoplanetary disks may act in concert with other mechanisms, such as the drag due to a disk wind emanating from deep in the disk (Miyake et al. 2015). However, here it important to note that the theory derived in this work applies to opaque grains, which also implies that to feel a photophoretic force they must have a size significantly greater than the wavelength of the thermal radiation in the disk.

The analysis of photophoresis driven dust motion in Section 3 treated only silicate dust. However grains made of other, such as graphite/organics, ices, or composites, all with different thermal properties, also populate protoplanetary disks; and can be expected to follow different protophoresis driven motions. This work motivates basic experiments to determine the appropriate parameters for these more diverse grain compositions.

We acknowledge enlightening conversations with Christophe Loesche and Gerhard Wurm on photophoresis driven by temperature fluctuations which lead to the concept behind this work. We thank the anonymous referee and Farrukh Naumann, and Melissa McClure for useful comments which improved the manuscript. The research leading to these results has received funding from the People Programme (Marie Curie Actions) of the European Union's Seventh Framework Programme (FP7/2007-2013) under REA grant agreement 327995 and ERC grant agreement

306614 (CPM), and NASA OSS grant NNX14AJ56G (AH).

APPENDIX

A. NUMERICAL SOLUTION TO SINGLE-LAYER SPHERE HEAT TRANSFER

To solve Equation (18) numerically we define the residual R as a function of the vector A of coefficents in the Legendre polynomial approximation:

$$R(A) \equiv k \left.\frac{\partial T}{\partial r}\right|_a + \sigma_{SB} T^4 - I_c(\theta) - I_n(\theta). \tag{70}$$

We then solve for A which minimizes the residual using a Levenberg-Marquardt least-squares algorithm. Typically we use 32 Legendre polynomials. To check the accuracy of the linear solution which has been expanded in $\eta \ll 1$ we wish to isolate the primary nonlinear term, with T^4, so we set the conductive cooling flux $I_c = 0$. Then, to analyze the relative error induced by the linear approximation,

$$\left(\frac{A_1 a}{A_0}\right)_{\text{linear}} \Big/ \left(\frac{A_1 a}{A_0}\right)_{\text{numerical}} - 1, \tag{71}$$

we need to only vary the parameters $\sigma_{SB} a/k$ and T_g. For dust motion in a protoplanetary disk, $T_g \in (0\,\text{K}, 10^4\,\text{K}]$, $\sigma_{SB} a/k \in [10^2, 10^9]$, and $\Gamma \in [0, 10^{-3}]$. Over these ranges we find that the relative error is always less than 10^{-6}, so the linear approximation to A_1 is excellent.

B. LINEAR SOLUTION TO DOUBLE-LAYER SPHERE HEAT TRANSFER

In the core and mantle layers, the temperature can be given in the series expansions:

$$T_c(\theta) = \sum_n \left(C_n r^n\right) P_n(\cos(\theta)), \tag{72}$$

$$T_m(\theta) = \sum_n \left(A_n r^n + B_n r^{-n-1}\right) P_n(\cos(\theta)). \tag{73}$$

The boundary conditions at the core radius r_c are

$$k_c \left.\frac{\partial T_c}{\partial r}\right|_{r_c} = k_m \left.\frac{\partial T_m}{\partial r}\right|_{r_c}, \tag{74}$$

$$T_c(r_c, \theta) = T_m(r_c, \theta), \tag{75}$$

where the second condition assumes that the interface has perfect conduction. At the outer, mantle plus core radius a, the boundary condition is

$$k_m \frac{\partial T_m}{\partial r} + 4\sigma_{SB} T_m^4 + \Upsilon T_g^{1/2}(T_g - T_2) = I_n(\theta). \tag{76}$$

Expanding the second left hand side term of Equation (76) and substituting the expansions in Equations (72) and (73) into the r_c and a boundary conditions leads to the following relations for the $n = 1$ coefficients:

$$k_c C_1 = k_m (A_1 - 2 r_c^{-3} B_1), \tag{77}$$

$$r_c C_1 = r_c A_1 + r_c^{-2} B_1, \tag{78}$$

$$k_m (A_1 - 2a^{-3} B_1) + 4\sigma_{SB} T_0^3 (a A_1 + a^{-2} B_1) - \Upsilon T_g^{1/2}(-a A_1 - a^{-2} B_1) = \sigma_{SB} T_g^4 \left(-\frac{8}{3}\Gamma\right). \tag{79}$$

The $n = 0$ terms yield $T_0 = T_g$ and $C_0 = A_0 + B_0 r_c^{-1}$. Solving the system of equations (77)–(79) yields the $n = 1$ coefficients in the T_m series:

$$\begin{aligned} A_1 a + B_1 a^{-2} = &- \frac{8}{3}\sigma_{SB} T_g^4 \Gamma \frac{a}{k_m}\left[(1 - b^3) + \frac{k_m}{k_c}(2 + b^3)\right] \\ &\times \left[2\frac{k_m}{k_c}(1 - b^3) + \left(1 + 2b^3\right) \right. \\ &\left. + \frac{a}{k_m}\left((1 - b^3) + \frac{k_m}{k_c}(2 + b^3)\right) \right. \\ &\left. \times \left(\Upsilon T_g^{1/2} + 4\sigma_{SB} T_g^3\right)\right]^{-1}, \end{aligned} \tag{80}$$

where $ab = r_c$. Using Equations (73) and (80), the approximate photophoresis force integral (Equation 5) yields

$$F_p \approx -\frac{\pi}{3}\alpha \frac{p}{T_g} a^2 (A_1 a + B_1 a^{-2}) \hat{\boldsymbol{e}}_z. \tag{81}$$

This completes the solution for the photophoresis force on the double-layered sphere.

REFERENCES

Beresnev, S., Chernyak, V., & Fomyagin, G. 1993, Physics of Fluids, 5, 2043
Blum, J., Wurm, G., Kempf, S., & Henning, T. 1996, Icarus, 124, 441
Ehrenhaft, F. 1918, Annalen der Physik, 361, 81
Friedrich, J. M., Weisberg, M. K., Ebel, D. S., Biltz, A. E., Corbett, B. M., Iotzov, I. V., Khan, W. S., & Wolman, M. D. 2014, ArXiv e-prints
Güttler, C., Blum, J., Zsom, A., Ormel, C. W., & Dullemond, C. P. 2010, A&A, 513, A56
Hayashi, C. 1981, Progress of Theoretical Physics Supplement, 70, 35
Hubbard, A. 2015, Icarus, 254, 56
Krause, M., Blum, J., Skorov, Y. V., & Trieloff, M. 2011, Icarus, 214, 286
Krauss, O., & Wurm, G. 2005, ApJ, 630, 1088
Loesche, C., & Wurm, G. 2012, A&A, 545, A36
Loesche, C., Wurm, G., McNally, C. P., Mac Low, M.-M., Hubbard, A., Teiser, J., Kelling, T., & Ebel, D. S. 2015, ApJ, Submitted
McNally, C. P., Hubbard, A., Yang, C.-C., & Mac Low, M.-M. 2014, ApJ, 791, 62
Miyake, T., Suzuki, T. K., & Inutsuka, S.-i. 2015, ArXiv e-prints
Moudens, A., Mousis, O., Petit, J.-M., Wurm, G., Cordier, D., & Charnoz, S. 2011, A&A, 531, A106
Mousis, O., Petit, J.-M., Wurm, G., Krauss, O., Alibert, Y., & Horner, J. 2007, A&A, 466, L9
Rohatscheck, H. 1995, J. Aerosol Sci., 26, 717
Rohatscheck, H., & Zulehner, W. 1985, J. of Colloid and Interface Sci., 108, 457
Rybicki, G. B., & Lightman, A. P. 1986, Radiative Processes in Astrophysics
Stoffels, W. W., Stoffels, E., Kroesen, G. M. W., & de Hoog, F. J. 1996, Journal of Vacuum Science Technology, 14, 588
Teiser, J., & Dodson-Robinson, S. E. 2013, A&A, 555, A98
Weidenschilling, S. J. 1977, MNRAS, 180, 57
Wurm, G., & Haack, H. 2009a, in Astronomical Society of the Pacific Conference Series, Vol. 414, Cosmic Dust - Near and Far, ed. T. Henning, E. Grün, & J. Steinacker, 509
Wurm, G., & Haack, H. 2009b, Meteoritics and Planetary Science, 44, 689
Wurm, G., Trieloff, M., & Rauer, H. 2013, ApJ, 769, 78